

See discussions, stats, and author profiles for this publication at: <https://www.researchgate.net/publication/51459927>

# Following Charge Separation on the Nanoscale in Cu<sub>2</sub>O-Au Nanoframe Hollow Nanoparticles

ARTICLE *in* NANO LETTERS · JULY 2011

Impact Factor: 13.59 · DOI: 10.1021/nl201642r · Source: PubMed

---

CITATIONS

70

READS

72

---

## 3 AUTHORS:



Mahmoud A. Mahmoud  
Georgia Institute of Technology

76 PUBLICATIONS 1,803 CITATIONS

[SEE PROFILE](#)



Wei Qian  
Georgia Institute of Technology

33 PUBLICATIONS 3,956 CITATIONS

[SEE PROFILE](#)



Mostafa A El-Sayed  
Georgia Institute of Technology

675 PUBLICATIONS 54,814 CITATIONS

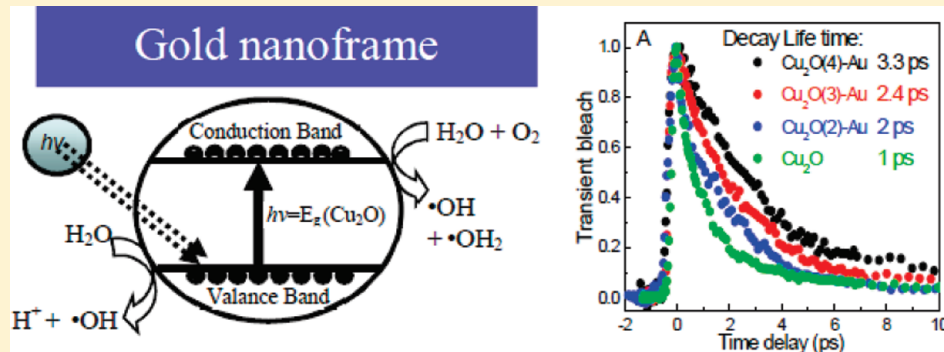
[SEE PROFILE](#)

# Following Charge Separation on the Nanoscale in Cu<sub>2</sub>O–Au Nanoframe Hollow Nanoparticles

Mahmoud A. Mahmoud, Wei Qian,<sup>†</sup> and Mostafa A. El-Sayed\*

Laser Dynamics Laboratory, School of Chemistry and Biochemistry, Georgia Institute of Technology, Atlanta, Georgia 30332-0400, United States

## ABSTRACT:



Cu<sub>2</sub>O–Au nanoframes with different nanolayer thicknesses of Cu<sub>2</sub>O were prepared, and their photocatalytic properties in aqueous solutions were studied. Cu<sub>2</sub>O semiconductor excitation leads to electron–hole separation. In aqueous solution, the hole is known to oxidize water to produce hydroxyl radicals whose concentration (and that of the holes) can be monitored by the rate of the degradation of dissolved methylene blue dye. The exciton lifetime is determined by femtosecond techniques and is determined by electron–hole recombination which depends on the rates of a number of competing processes such as, electron or hole transfer to an acceptor such as a gold nanoframe and/or the electron or hole trapping processes at the Cu<sub>2</sub>O–Au nanoframe interface. We measured the exciton lifetime as a function of the average Cu<sub>2</sub>O–Au layer separation. A good correlation was found between the rate of the photocatalytic degradation of methylene blue and the exciton lifetime. The exciton lifetime is found to increase as the Cu<sub>2</sub>O thickness is increased. This leads to an increase in the electron–hole separation time and thus an increase in the hole (and so the hydroxyl radical) concentration leading to an observed enhanced rate of the dye degradation.

**KEYWORDS:** Photocatalysis, electron and hole separation, femtosecond dynamics, cuprous oxide, nanoframe, gold

It is known that photoexcited semiconductor metal oxides photocatalyze the degradation of organic dyes very efficiently in aqueous solutions.<sup>1,2</sup> This results from the separation of the electrons and holes within the semiconductor.<sup>1</sup> The holes oxidize water into •OH radicals which attack the double bonds of dissolved dye molecules, hereby destroying the dye and bleaching its color.<sup>2–4</sup> This technique is used to destroy azo dyes, which are used in the textile industry and are toxic to the environment. The electron if separated from the holes within the semiconductor can be used to reduce water into H<sub>2</sub> gas.<sup>5</sup>

Cu<sub>2</sub>O is a p-type semiconductor with band gap of 2.0–2.2 eV.<sup>6</sup> It has been used for solar energy conversion due to its absorption in the visible region.<sup>2</sup> In addition to solar energy conversion, Cu<sub>2</sub>O has been used as a photocatalyst for the electrochemical splitting of water using visible light irradiation and the degradation of organic materials.<sup>6–9</sup> Cu<sub>2</sub>O has been successfully synthesized by many methods including electrolysis,<sup>10</sup> reduction of cupric salts or cupric oxide, thermal oxidation of copper,<sup>11</sup> hydrothermal production, and  $\gamma$ -irradiation of cupric salt.<sup>12</sup>

The band gap of Cu<sub>2</sub>O, like most of semiconductor materials, can be tuned by changing the size of the Cu<sub>2</sub>O particles. This

property makes Cu<sub>2</sub>O, useful not only as a photocatalyst but also as a semiconductor photosensitizer for solar cells.<sup>13,14</sup> Cu<sub>2</sub>O showed low toxicity as well as good environmental acceptability. It is also more available at a reasonable cost, compared to many other semiconductors.<sup>15</sup> One of the advantages of Cu<sub>2</sub>O as a photocatalyst is its ability to strongly adsorb molecular oxygen, which can scavenge photoelectrons and thus minimize electron–hole recombination.<sup>16</sup> If the holes are not scavenged properly, Cu<sub>2</sub>O is oxidized to CuO which could affect the efficiency of Cu<sub>2</sub>O as a photocatalyst. However it has been reported that the Cu<sub>2</sub>O surface can be stabilized by a controlled oxidation and the formation of a thin protecting film of CuO.<sup>17</sup> Some studies showed that Cu<sub>2</sub>O nanoparticles with sizes less than 25 nm are more stable than CuO.<sup>18</sup> The photocatalytic splitting of water on Cu<sub>2</sub>O powder has been shown to proceed without any noticeable deactivation for more than 1900 h.<sup>7</sup> It has been reported that Cu<sub>2</sub>O does not exist as a bulk in ambient atmosphere, but on the

**Received:** May 16, 2011

**Revised:** June 28, 2011

**Published:** July 01, 2011

nanoscale it becomes substantially stable.<sup>19</sup> Cu<sub>2</sub>O nanoparticles with octahedron shapes of different sizes has been used in the photocatalytic decomposition of methyl orange.<sup>20</sup>

In the present study, a novel method was used to synthesize a cuprous oxide/gold nanoframe to separate the electrons from the holes. The system is a Au hollow nanoframe of fixed wall thickness whose surfaces are covered with a shell of Cu<sub>2</sub>O of varying thicknesses. In an aqueous solution containing these nanoparticles, we measured the rates of two processes: (1) The rate of disappearance of the color of methylene blue dye (MB), which presumably is sensitive to the hole concentration, and (2) the Cu<sub>2</sub>O exciton decay time by using femtosecond spectroscopy. The latter is found to be dependent on the Cu<sub>2</sub>O thickness, i.e., the average Cu<sub>2</sub>O to gold nanoshell separation. The exciton lifetime can be tuned by changing the Cu<sub>2</sub>O thickness and subsequently be used to examine the change in the rate of the dye color change. The more efficiently the electrons and holes are separated, the higher the hole concentration becomes and the more efficiently an environmentally polluting dye can be destroyed (this also should result in a higher nanophotocurrent and H<sub>2</sub> gas production from the nanoframe cavity nanosystem which were not studied in the present work). The rate of the disappearance of the methylene blue dye in solution and the exciton decay in the photoexcited Cu<sub>2</sub>O are both measured as a function of the thickness of Cu<sub>2</sub>O, which controls the Cu<sub>2</sub>O–Au coupling and thus the efficiency of charge separation. In order to understand the role of gold in enhancing the electron–holes separation and the photocatalytic properties of Cu<sub>2</sub>O, pure Cu<sub>2</sub>O nanospheres are prepared and the photocatalytic and dynamic properties are studied and compared with the core–shell system.

**Experimental Section.** Gold nanoframes (AuNFs), 80 nm, were prepared from silver nanocubes (AgNCs) by galvanic replacement as described in our previous work.<sup>21</sup> The SPR peak position of the AuNF is at 1030 nm. One hundred milliliters of the prepared AuNFs were precipitated by centrifugation and redispersed in 30 mL of deionized (DI) water. In order to coat walls of the AuNFs with different thicknesses of Cu<sub>2</sub>O, 5 mL of AuNFs was injected into a cupric chloride (CuCl<sub>2</sub>·2H<sub>2</sub>O) solution.<sup>22</sup> Four CuCl<sub>2</sub>·2H<sub>2</sub>O solutions were prepared by dissolving 0.5 g of PVP (MW ~55000 g) and 5, 6, 7, and 8 mg of CuCl<sub>2</sub>·2H<sub>2</sub>O, respectively in 80 mL of DI water with stirring. These solutions have an acidic pH value. To increase the pH of the solutions, 0.01 M sodium hydroxide was added dropwise with constant low speed stirring until the pH became ~8.5. The final volume of the solution was brought to 100 mL by addition of DI water. The stirring was continued for another 2 min at pH = 8.5. Under these conditions, a cupric hydroxide layer was deposited onto the surface of AuNFs. Finally, 4 mL of 0.1 hydrazine hydrate (N<sub>2</sub>H<sub>4</sub>·H<sub>2</sub>O) was added with constant stirring. The stirring continued for 5 min to reduce the cupric hydroxide into cuprous hydroxide. The resulting solutions were heated (in an oil bath) at 45 °C for 1 h with constant stirring to decompose the cuprous hydroxide layer coating the AuNF into Cu<sub>2</sub>O. Samples containing 5, 6, 7, and 8 mg of CuCl<sub>2</sub>·2H<sub>2</sub>O are herein referred to Cu<sub>2</sub>O(1)-Au, Cu<sub>2</sub>O(2)-Au, Cu<sub>2</sub>O(3)-Au, and Cu<sub>2</sub>O(4)-Au nanoframes, respectively. Similar steps were used with little modification for the synthesis of Cu<sub>2</sub>O nanospheres; the weight of CuCl<sub>2</sub>·2H<sub>2</sub>O was increased to 17 mg, 8 mL of N<sub>2</sub>H<sub>4</sub>·H<sub>2</sub>O was used, and no AuNFs were added. A Carry UV–vis–NIR (Cary 500, Version 8.01) used to measure the optical spectra. A JEOL 100C transmission electron microscope was used to characterize the synthesized particles.

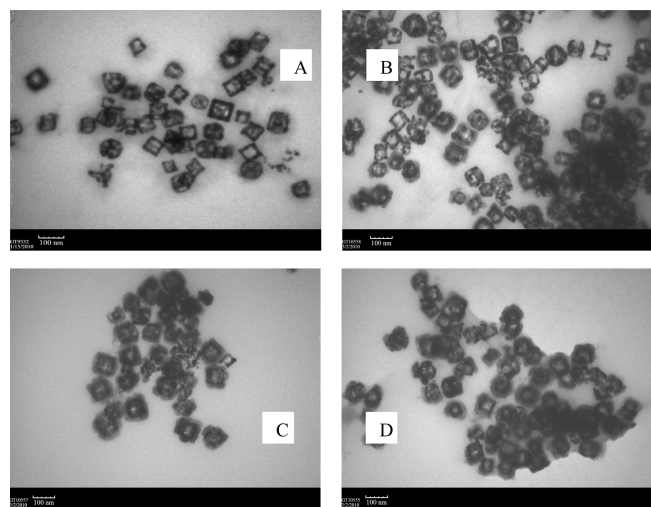


**Figure 1.** TEM images of 80 nm Cu<sub>2</sub>O-Au nanoframe of different thickness, the thickness increases in this order Cu<sub>2</sub>O(1)-Au (A), Cu<sub>2</sub>O(2)-Au (B), Cu<sub>2</sub>O(3)-Au (C), and Cu<sub>2</sub>O(4)-Au nanoframes (D). The scale bars are 100 nm.

Before the photocatalysis experiments are carried out, the extra PVP capping material was removed from the Cu<sub>2</sub>O–Au nanoframes and pure Cu<sub>2</sub>O nanocatalysts by centrifuging them at 8000 rpm and redisperse in DI water twice. Then the concentration of copper in each solution was determined via ICP-MS. On the basis of the concentration of copper in each solution of the catalysts, deionized water was added to each catalyst to make the amount of the Cu<sub>2</sub>O per unit volume in each solution equal. In a 4 mL quartz cuvette with a long neck, 0.5 mL of the Cu<sub>2</sub>O/Au nanocatalyst solution is added to 0.3 mL of 100 ppm methylene blue (MB). The final volume of the solution was diluted to 3.5 mL by addition of DI water. The resulting solution was irradiated with a 40 W xenon lamp equipped with a UV filter. The reduction in the optical absorption peak of MB was determined from the UV–vis spectrum by using an Ocean optics HR4000Cg-UV-NIR spectrometer. For the dynamic decay measurements a femtosecond system was used which involves a frequency-doubled Nd:vanadate laser (Coherent Verdi) to pump a Ti–sapphire laser (Clark MXR CPA 1000) to obtain 800 nm pulses of 100 fs duration and 1 mJ energy per pulse with a 1 kHz repetition rate. The 800 nm pulses were frequency doubled by using a BBO crystal to produce 400 nm pump pulses. Most of this pulse is used to pump the sample, while only 40 μJ passes through a sapphire plate, generating a femtosecond white light continuum in the range of 400–1100 nm which is used as a probe beam. The pump and probe beams are then cofocused onto the sample. The sample was placed in a quartz cuvette having a cross section of 1 mm. Transient absorption spectra at 460 nm were monitored using a monochromator/photodiode arrangement coupled to a boxcar integrator and a lock-in amplifier (Stanford Research System SR 530).

**Results and Discussion. Photocatalyst Characterization.** The optical, electrical, physical, and catalytic properties of nanoparticles depend on their shape and size. However, in order to study any of these properties of the nanoparticles and before using them in any application, they should be imaged and characterized. The characterization techniques such as transmission electron microscopy (TEM) and scanning electron microscopy (SEM) are based on electron beam interaction with the nanoparticles. Figure 1 shows the TEM images of Cu<sub>2</sub>O(1)-Au, Cu<sub>2</sub>O(2)-Au, Cu<sub>2</sub>O(3)-Au,

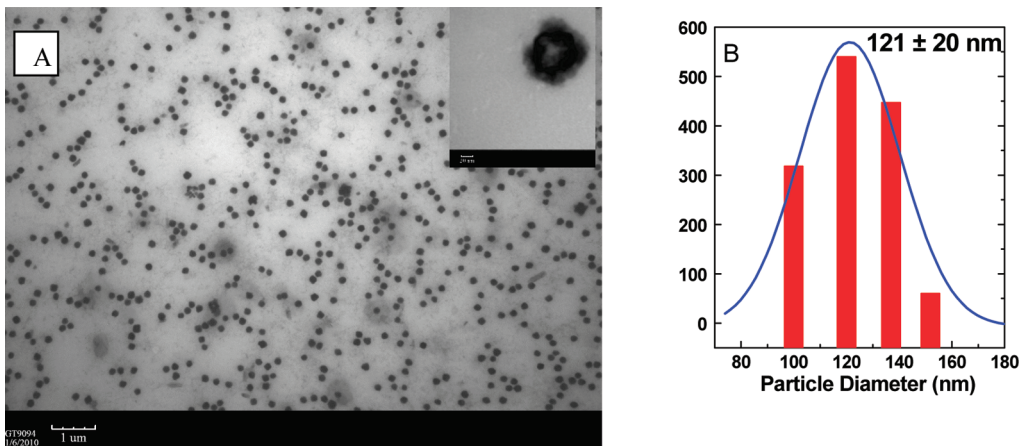


**Figure 2.** (A) TEM of Cu<sub>2</sub>O nanoparticles, the inside panel is a magnified single Cu<sub>2</sub>O nanoparticle; the scale bar of the magnified Cu<sub>2</sub>O in the panel inside is 20 nm. (B) Size distribution of Cu<sub>2</sub>O hollow nanospheres fitted to Gaussian; the particle size is 121 ± 20 nm.

and Cu<sub>2</sub>O(4)-Au nanoframes. From the images we observe that Cu<sub>2</sub>O coated the walls of the AuNFs, the cavity inside the frame is still open, and the Cu<sub>2</sub>O distribution is uniform. Moreover, the thickness of the Cu<sub>2</sub>O increases as the amount of copper salt added increases (as shown in the Experimental Section). The wall length of these particles is 80 nm and the wall thickness is ~3–6 nm, depending on the amount of copper salt added during the synthesis method.

In order to prepare Cu<sub>2</sub>O nanospheres; Cu(OH)<sub>2</sub> nanoparticles are prepared first which are reduced with hydrazine hydrate to CuOH and then decompose into Cu<sub>2</sub>O and water.<sup>23</sup> Figure 2A shows the TEM image of Cu<sub>2</sub>O sphere nanoparticle, while a magnified Cu<sub>2</sub>O nanosphere is shown in the inset panel. Figure 2B shows the size distribution fit to a Gaussian function; the particle size of a Cu<sub>2</sub>O nanosphere is 121 ± 20 nm.

X-ray photoelectron spectroscopy (XPS) is a useful technique for analyzing the elemental constituents of nanoparticles and nanocomposites. The XPS spectrum assists in the determination of the oxidation state of the elements as well as whether the material examined is in a pure or alloy form. Figure 3 shows the XPS spectrum of the Cu<sub>2</sub>O(4)-Au nano-frame. The single peak at 935.5 eV corresponds to the presence of Cu<sup>+</sup> 2p<sub>3/2</sub>, confirming the presence of Cu<sub>2</sub>O. The tail around 937.5 eV is due to the presence of a layer of CuO on the top of a Cu<sub>2</sub>O nanolayer.<sup>24,25</sup> Cu<sup>2+</sup>, like other d<sup>9</sup> ground state electronic configuration materials, has two characteristic broad XPS peaks in addition to the main phase at higher binding energies.<sup>25</sup> In our case, they are connected together and are centered on 944 eV.

**Surface Plasmon Resonance Spectrum of Au–Cu<sub>2</sub>O Nano-frame with Different Cu<sub>2</sub>O Thicknesses.** Plasmonic nanoparticles are characterized by surface plasmon resonance (SPR), which is accompanied with an electromagnetic plasmon field. The SPR peak position and the plasmon field intensity depend on the shape and size of the nanoparticles as well as the dielectric of the surrounding medium.<sup>26</sup> AuNFs have a plasmon peak in the NIR region, in addition to a plasmon field inside and outside the nanoframe walls.<sup>21,26,27</sup> The SPR peak red shifts as the frame wall thickness decreases.<sup>26</sup> Eighty nanometer AuNFs with wall thickness of 16 nm has a SPR peak centered at 1030 nm in aqueous medium,<sup>21</sup> and after coating with the Cu<sub>2</sub>O layer, the SPR redshifts to 1200 nm due to the change of the dielectric constant of

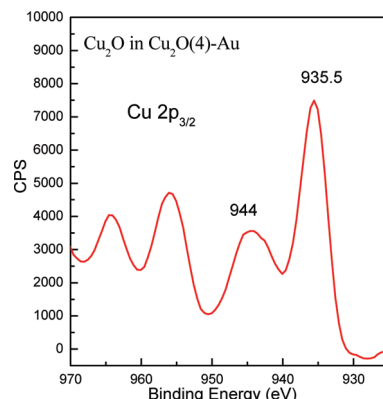


**Figure 3.** XPS spectrum of Cu 2p<sub>3/2</sub> of Cu<sub>2</sub>O(4)-Au nano-frame. The spectrum and the analysis show the presence of both Cu<sub>2</sub>O and a small amount of CuO.

the surroundings (see Figure 4). On increase of the amount of Cu<sub>2</sub>O deposited on the walls of AuNF, the SPR peak position does not show much shift. Figure 4 shows the optical spectra of Cu<sub>2</sub>O(1)-Au, Cu<sub>2</sub>O(2)-Au, Cu<sub>2</sub>O(3)-Au, Cu<sub>2</sub>O(4)-Au, and Cu<sub>2</sub>O. The SPR peak intensities are comparable in the four samples, while the intensity of the absorption peaks at 350 and 450 nm of Cu<sub>2</sub>O increases as its thickness increases. The pure spherical shape Cu<sub>2</sub>O nanoparticle has an extinction peak with maximum at 478 nm.

**Photocatalysis of Methylene Blue by Cu<sub>2</sub>O–Au Nanoframes: Effect of Cu<sub>2</sub>O Thickness.** Photocatalysis has been shown to produce free radicals.<sup>2,28,29</sup> Previous studies on the photocatalytic degradation of organic dyes showed that the reaction proceeds through the formation of •OH and •OOH radicals.<sup>2,4</sup> Those radicals attack the organic dyes and cause the photodissociation. In fact, •OH and •OOH have not been isolated due to their ultrashort lifetime, but hydroxy intermediate compounds have been detected during the photodissociation.<sup>28</sup> It has been reported that Cu<sub>2</sub>O absorbs visible light and cause the photodegradation of MB.<sup>30</sup> The proposed mechanism for this reaction is based on the formation of a hydroxyl radical that results from the photodissociation of water. Here we compare the efficiencies of Cu<sub>2</sub>O-Au nanoparticles of different thicknesses and having internal Au surfaces with pure Cu<sub>2</sub>O nanoparticles. We used the

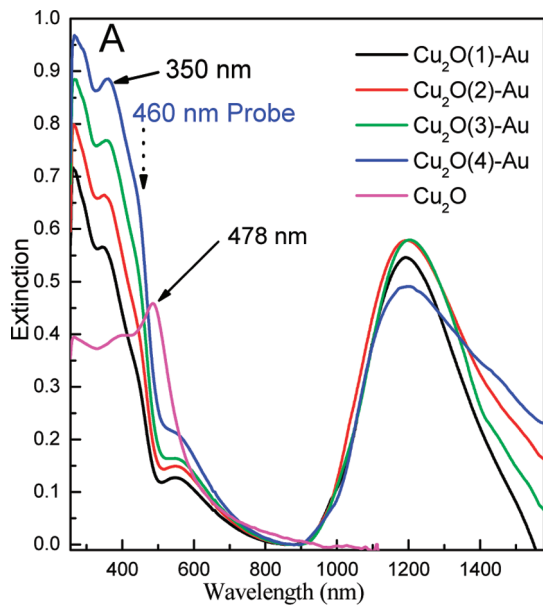


**Figure 4.** The extinction spectra of AuNF coated with different thickness of  $\text{Cu}_2\text{O}$ . The thickness of  $\text{Cu}_2\text{O}$  increases in the order of  $\text{Cu}_2\text{O}(1)\text{-Au}$ ,  $\text{Cu}_2\text{O}(2)\text{-Au}$ ,  $\text{Cu}_2\text{O}(3)\text{-Au}$ , and  $\text{Cu}_2\text{O}(4)\text{-Au}$  nanoframes, respectively. Absorption spectrum of pure  $\text{Cu}_2\text{O}$  nanospheres (magenta color).

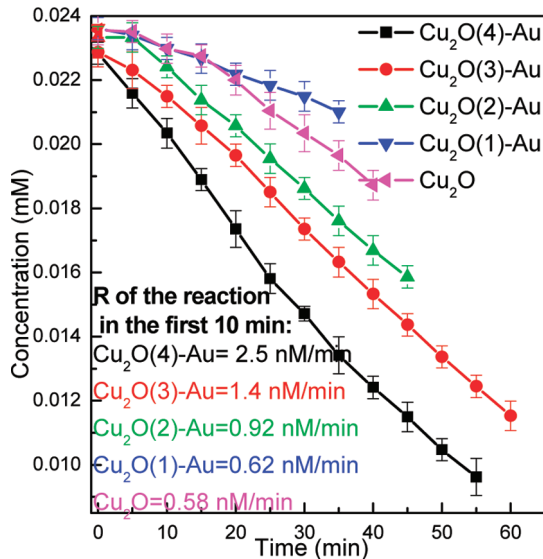


**Figure 5.** The effect of photochemically excited  $\text{Cu}_2\text{O}$  nanospheres and  $\text{Cu}_2\text{O}$  with different thicknesses, coated a constant shell thickness of Au shell on the rate of photocatalytic destruction of MB in solution. The initial rate is found to increase by increasing the  $\text{Cu}_2\text{O}$  thickness.

rate of the photodegradation of MB as a measure of the efficiency of these prepared nanocatalysts in producing  $\cdot\text{OH}$  radicals and which give a measure of the efficiency of hole production. The rate of photodegradation of MB by pure  $\text{Cu}_2\text{O}$  nanoparticles is used to monitor the effect of gold on the efficiency of  $\text{Cu}_2\text{O}$  in  $\text{Cu}_2\text{O}\text{-Au}$  system. In fact, a Schottky barrier was assumed to form at the gold– $\text{Cu}_2\text{O}$  interface; however gold acts as an electron sink that reduces the recombination of photoinduced electrons and holes.<sup>4</sup>

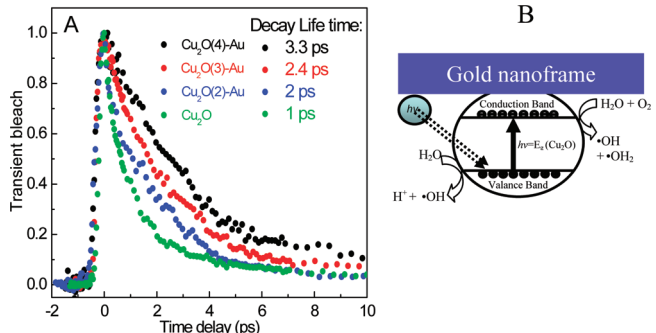


**Figure 6.** (A) The transient bleach intensity as a function of delay time for pump wavelength at 400 nm and probe at 460 nm. The decay curves result from the exciton relaxation at electron hole recombination and transfer to the gold and to the defects at its interface. Faster decay is observed for thinner  $\text{Cu}_2\text{O}$  samples or smaller  $\text{Cu}_2\text{O}$ –Au separation. (B) Schematic diagram summarizing the excitation of  $\text{Cu}_2\text{O}$  by visible light and the mechanism of radical formation.

MB has a sharp optical absorption peak around 664 nm. The decrease in this absorption peak intensity is used to follow the photodissociation kinetics of MB, which depends on the  $\cdot\text{OH}$  radical concentration, which itself depends on the  $\text{Cu}_2\text{O}$  hole concentration. Therefore, we assume that the efficiency of the  $\text{Cu}_2\text{O}$  photocatalyst depends on the steady state concentration of its holes, which in turns depends on the efficiency of the charge separation between the holes and electrons. Since holes drive the free radical photochemical reaction, we can monitor the electron–hole separation efficiency in the  $\text{Cu}_2\text{O}$  by following the hole via the photocatalytic degradation of MB. Figure 5 shows the relationship between the concentration of MB (in mM) and the reaction time (in minutes). The initial rate is a measure of the hole concentration produced in the photoexcitation of the different  $\text{Cu}_2\text{O}$ –Au nanoframe and pure  $\text{Cu}_2\text{O}$  nanospheres systems. The photodissociation reaction rate is relatively slow. The change in the concentration of MB in the first 10 min of the reaction is used as the initial rate of the reaction. This is found to be 2.5, 1.4, 0.92, 0.62, and 0.58 nM/min for  $\text{Cu}_2\text{O}(4)\text{-Au}$ ,  $\text{Cu}_2\text{O}(3)\text{-Au}$ ,  $\text{Cu}_2\text{O}(2)\text{-Au}$ ,  $\text{Cu}_2\text{O}(1)\text{-Au}$ , and pure  $\text{Cu}_2\text{O}$  photocatalysts, respectively. The rate of the photocatalytic reaction is found to increase as the thickness of the  $\text{Cu}_2\text{O}$  increases, and gold increases the rate of photocatalytic reaction and so the hole concentration.

**Exciton Lifetimes of the  $\text{Cu}_2\text{O}$  in  $\text{Cu}_2\text{O}$ –Au Nanoframe of Different  $\text{Cu}_2\text{O}$  Shell Thicknesses.** Time-resolved optical techniques have been used to study the charge carrier dynamics as a function of the thickness of the  $\text{Cu}_2\text{O}$  frame using a femtosecond pump–probe technique.<sup>31</sup> Figure 6A shows the transient bleach decay as a function of the delay time between the pump at 400 nm and the probe at 460 nm. The relaxation of the excitation of  $\text{Cu}_2\text{O}$  at 460 nm has been fitted to a single exponential decay and the lifetime was found to be 3.3, 2.4, 2, and 1 ps for  $\text{Cu}_2\text{O}(4)\text{-Au}$ ,  $\text{Cu}_2\text{O}(3)\text{-Au}$ , and  $\text{Cu}_2\text{O}(2)\text{-Au}$  nanoframes and  $\text{Cu}_2\text{O}$  nanosphere, respectively. The lifetime of the hot electrons increases with increasing the thickness of the  $\text{Cu}_2\text{O}$  nanoshell layer, while it decreases in the absence of gold as in pure  $\text{Cu}_2\text{O}$  nanospheres.

When  $\text{Cu}_2\text{O}$  interacts with electromagnetic radiation, an electron is transferred from the valence to the conduction band, generating a hole in the valence band. The observed decay is not exponential suggesting the presence of more than one channel in

competition with the electron and hole recombination such as defect trapping, electron or hole transfer to the gold. These processes compete with the electron–hole recombination thereby increasing the hole lifetime and thus its concentration which result in an increase in the radical concentration and a faster rate of the color photobleach of the MB. The fact that the overall decay rate of the exciton decreases with decreasing the thickness of the Cu<sub>2</sub>O might suggest that both the rate of the energy transfer to the gold and the defect trapping process occur at the Cu<sub>2</sub>O–Au nanoframe interface as physically expected. Figure 6B summarizes the radical formation based on the dynamic studies. Pure Cu<sub>2</sub>O nanoparticles have the shortest lifetime decay compared with the Cu<sub>2</sub>O–Au nanoframe system. The reason is that there is no gold there to scavenge the electrons and so the lifetime of electron–hole recombination is prolonged.

**Conclusion.** In Cu<sub>2</sub>O–Au nanoframes with different Cu<sub>2</sub>O layer thickness, both the exciton decay time of the Cu<sub>2</sub>O semiconductor and its photodegradation rate of MB dye in aqueous solution are found to increase as the thickness of the Cu<sub>2</sub>O increases. These results can be understood if the lifetime of the excitation of the electron and hole is determined by the energy transfer to the gold or gold–Cu<sub>2</sub>O interface defects, the rate of which depends on the thickness of the Cu<sub>2</sub>O frame. The faster the transfer (e.g., for thin Cu<sub>2</sub>O frame), the more efficient the electron–hole separation becomes and the faster the rate of the dye degradation.

## ■ AUTHOR INFORMATION

### Corresponding Author

\*E-mail: melsayed@gatech.edu.

### Current Address

<sup>†</sup>IMRA America, Inc., 1044 Woodridge Ave., Ann Arbor, Michigan 48105, United States.

## ■ ACKNOWLEDGMENT

This work was supported by the NSF Grant No. 0957335. The authors wish to thank Ms Rachel Near for her careful proofreading of the manuscript.

## ■ REFERENCES

- (1) Fujishima, A.; Honda, K. *Nature* **1972**, 238, 37.
- (2) Badr, Y.; Mahmoud, M. A. *J. Phys. Chem. Solids* **2007**, 68, 413.
- (3) Badr, Y.; El-Wahed, M. G. A.; Mahmoud, M. A. *J. Hazard. Mater.* **2008**, 154, 245.
- (4) Lu, W. W.; Gao, S. Y.; Wang, J. *J. Phys. Chem. C* **2008**, 112, 16792.
- (5) Sokmen, M.; Allen, D. W.; Akkas, F.; Kartal, N.; Acar, F. *Water, Air, Soil Pollut.* **2001**, 132, 153.
- (6) Fernando, C. A. N.; de Silva, P. H. C.; Wethasinha, S. K.; Dharmadasa, I. M.; Delsol, T.; Simmonds, M. C. *Renewable Energy* **2002**, 26, 521.
- (7) Hara, M.; Kondo, T.; Komoda, M.; Ikeda, S.; Shinohara, K.; Tanaka, A.; Kondo, J. N.; Domen, K. *Chem. Commun.* **1998**, 357.
- (8) Ikeda, S.; Takata, T.; Kondo, T.; Hitoki, G.; Hara, M.; Kondo, J. N.; Domen, K.; Hosono, H.; Kawazoe, H.; Tanaka, A. *Chem. Commun.* **1998**, 2185.
- (9) Senevirathna, M. K. I.; Pitigala, P.; Tennakone, K. *J. Photochem. Photobiol. A* **2005**, 171, 257.
- (10) Golden, T. D.; Shumsky, M. G.; Zhou, Y. C.; VanderWerf, R. A.; VanLeeuwen, R. A.; Switzer, J. A. *Chem. Mater.* **1996**, 8, 2499.
- (11) Musa, A. O.; Akomolafe, T.; Carter, M. J. *Sol. Energy Mater. Sol. Cells* **1998**, 51, 305.
- (12) Zhu, Y. J.; Qian, Y. T.; Zhang, M. W.; Chen, Z. Y.; Xu, D. F.; Yang, L.; Zhou, G. *Mater. Res. Bull.* **1994**, 29, 377.
- (13) Lu, C. H.; Qi, L. M.; Yang, J. H.; Wang, X. Y.; Zhang, D. Y.; Xie, J. L.; Ma, J. M. *Adv. Mater.* **2005**, 17, 2562.
- (14) Katayama, J.; Ito, K.; Matsuoka, M.; Tamaki, J. *J. Appl. Electrochem.* **2004**, 34, 687.
- (15) Siripala, W.; Ivanovskaya, A.; Jaramillo, T. F.; Baeck, S. H.; McFarland, E. W. *Sol. Energy Mater. Sol. Cells* **2003**, 77, 229.
- (16) Li, J. L.; Liu, L.; Yu, Y.; Tang, Y. W.; Li, H. L.; Du, F. P. *Electrochem. Commun.* **2004**, 6, 940.
- (17) Borgohain, K.; Murase, N.; Mahamuni, S. *J. Appl. Phys.* **2002**, 92, 1292.
- (18) Zhu, H. Juny. *Phys. Rev. B* **1996**, 53, 2167.
- (19) Ram, S.; Mitra, C. *Mater. Sci. Eng., A* **2001**, 304, 805.
- (20) Xu, H. L.; Wang, W. Z.; Zhu, W. *J. Phys. Chem. B* **2006**, 110, 13829.
- (21) Mahmoud, M. A.; El-Sayed, M. A. *Nano Lett.* **2009**, 9, 3025.
- (22) Kuo, C. H.; Hua, T. E.; Huang, M. H. *J. Am. Chem. Soc.* **2009**, 131, 17871.
- (23) Kuo, C. H.; Chen, C. H.; Huang, M. H. *Adv. Funct. Mater.* **2007**, 17, 3773.
- (24) Wu, C. K.; Yin, M.; O'Brien, S.; Koberstein, J. T. *Chem. Mater.* **2006**, 18, 6054.
- (25) Chusuei, C. C.; Brookshier, M. A.; Goodman, D. W. *Langmuir* **1999**, 15, 2806.
- (26) Mahmoud, M. A.; El-Sayed, M. A. *J. Am. Chem. Soc.* **2010**, 132, 12704.
- (27) Mahmoud, M. A.; Snyder, B.; El-Sayed, M. A. *J. Phys. Chem. C* **2010**, 114, 7436.
- (28) Comparelli, R.; Fanizza, E.; Curri, M. L.; Cozzoli, P. D.; Mascolo, G.; Passino, R.; Agostiano, A. *Appl. Catal., B* **2005**, 55, 81.
- (29) Wang, Z. H.; Zhao, S. P.; Zhu, S. Y.; Sun, Y. L.; Fang, M. *CrystEngComm* **2011**, 13, 2262.
- (30) Zhu, H.; Zhang, J.; Lan, X.; Li, C.; Wang, T.; Huang, B. *Mater. Sci. Forum* **2009**, 610–613, 293.
- (31) Lou, Y.; Yin, M.; O'Brien, S.; Burda, C. *J. Electrochem. Soc.* **2005**, 152, G427.